ACS APPLIED ELECTRONIC MATERIALS

pubs.acs.org/acsaelm Article

High Performance Indium-Tin-Zinc-Oxide Thin-Film Transistor with Hexamethyldisilazane Passivation

Xinkai Sun,[‖] Jae-Hoon Han,[‖] Zhenyuan Xiao, Simin Chen, Taewon Jin, Taehyeon Noh, Seoungmin Park, Jaekyun Kim, Jidong Jin,* and Younghyun Kim*

Cite This: *ACS Appl. Electron. Mater.* 2024, 6, 2442−2448 Read Online

ACCESS | Metrics & More | Article Recommendations | Supporting Information

ABSTRACT: In this work, the fabrication and characterization of high performance indium-tin-zinc-oxide (ITZO) thin-film transistors (TFTs) with hexamethyldisilazane (HMDS) passivation are presented. The incorporation of HMDS passivation significantly enhances the electrical performance and bias stress stability of ITZO TFTs compared with those without HMDS passivation. X-ray photoelectron spectroscopy measurements reveal that ITZO TFTs with HMDS passivation offer distinct advantages over those without HMDS passivation, including an increased concentration of metal oxide and a reduced concentration of oxygen vacancies and hydroxyl groups in the active channel layer. As a result, the ITZO TFTs with HMDS passivation exhibit a saturation mobility of 26.15 ± 1.14 $cm^2 \cdot V^{-1} \cdot s^{-1}$, a subthreshold swing of 0.26 ± 0.04 $V \cdot dec^{-1}$, an on/off current ratio of 9×10^8, and excellent operational bias stress stability when compared to ITZO TFTs without HMDS passivation.

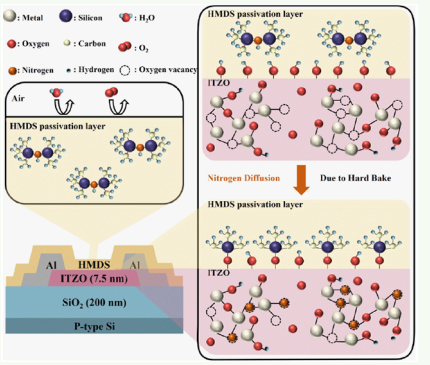

KEYWORDS: *indium tin zinc oxide (ITZO), thin-film transistors (TFTs), hexamethyldisilazane (HMDS) passivation, bias stress stability*

1. INTRODUCTION

Oxide semiconductor thin-film transistors (TFTs) have been extensively investigated for their potential in next-generation display applications.[1−6] To achieve displays with high resolution, oxide semiconductor TFTs must have high field-effect mobility and excellent bias stress stability.[4,7] Recently, indium-tin-zinc-oxide (ITZO) TFTs have drawn significant interest due to their high field-effect mobility, high transparency, and processability at low temperature.[7−13] However, instability under bias stress remains a critical challenge for ITZO TFTs.[14,15] It has been reported that this instability is closely linked to oxygen-related defects within the ITZO active layers, such as oxygen vacancies and hydroxyl groups.[10] Thermal annealing is widely employed to control defects and enhance the stability issues of ITZO TFTs.[10,12,16] Furthermore, the ITZO active channel layer is highly susceptible to oxygen and moisture in the air, which can lead to severe instability issues under bias stress.[14,17] Therefore, a dual active channel layer or a surface passivation layer is generally required to serve as a barrier, isolating the ITZO active layer from oxygen and moisture in the air, thereby significantly enhancing the stability of ITZO TFTs.[10,12,14,18−21]

Various passivation layers, such as SiO_2, Y_2O_3, Sc_2O_3, HfO_2, and Al_2O_3 have been investigated as potential solutions to solve the instability issues in oxide semiconductor TFTs.[9,21−25] However, most of these passivation layers are typically deposited using conventional chemical and physical vapor deposition techniques, which generally require a high vacuum or an inert gas atmosphere, both of which are generated at considerable expense. To overcome these constraints, research has turned its focus toward solution-processed passivation layers, preferred for simplicity of deposition and cost-effectiveness.[15,23,26] Hexamethyldisilazane (HMDS) is one of the silane reagents that can be deposited by solution processing and reacted with an oxidized surface to form a highly hydrophobic surface.[27] Consequently, HMDS is widely used in the fields of biology and material protection, especially in semiconductor applications such as surface treatments for organic semiconductor TFT insulators.[27,28] Nevertheless, the application of HMDS as a passivation layer in oxide semiconductor TFTs remains unexplored.

In this work, the use of HMDS passivation layers for ITZO TFTs is introduced, employing a solution-based deposition method. ITZO TFTs are fabricated both with and without HMDS passivation layers, revealing that HMDS passivation leads to significant enhancements in the electrical properties and stability of the TFTs compared to those without it.

Received: January 17, 2024
Revised: March 6, 2024
Accepted: March 28, 2024
Published: April 10, 2024

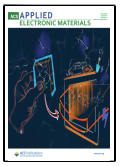

https://doi.org/10.1021/acsaelm.4c00100
ACS Appl. Electron. Mater. 2024, 6, 2442−2448

2. EXPERIMENTAL DETAILS

2.1. Device Fabrication. Heavily doped p-type Si with a 200-nm-thick thermally oxidized SiO_2 was used as the substrate. First, the SiO_2 gate insulator was patterned by photolithography and wet etching to form a gate via. Then, a 7.5-nm-thick channel layer of ITZO was deposited onto the SiO_2/Si substrate by using radio frequency (RF) sputtering. The sputtering process employed an ITZO target ($In_2O_3/SnO_2/ZnO$ = 4:1:4 mol %) with an RF power of 25 W, a working pressure of 7.5 mTorr, and an Ar gas input flow rate of 45 sccm. Next, thermal annealing of the ITZO active layers was conducted at 290 °C in air for 1 h to reduce oxygen-related defects and the increase of carrier concentration.[16] Subsequently, 50-nm-thick aluminum (Al) source/drain (S/D) electrodes were deposited by thermal evaporation. The length (L) and width (W) of the channel were 20 and 100 μm, respectively. Finally, the passivation layer was formed by spin-coating the HMDS solution for 20 s at 1000 rpm under ambient room temperature conditions, followed by a 3 min bake at 113 °C to evaporate the remaining solvent and fully cure the HMDS passivation layer. The device fabrication process and an optical image of a fabricated ITZO TFT with HMDS passivation are shown in Figure S1.

2.2. Film and Device Characterization. The grazing incidence X-ray diffraction (GIXRD) pattern of the ITZO film was obtained using a Bruker D8 Advance system. The optical band gap of the ITZO film was determined by measuring its absorption spectrum by using a Cary 5000 ultraviolet visible near-infrared (UV−vis−NIR) spectrophotometer. Static contact angles were measured with a First Ten Angstroms FTA1000 Contact Angle Analyzer. The film morphology was examined by using a Bruker Multimode 8 atomic force microscopy (AFM) system. Changes in the chemical states within the active channel layers were investigated by using a Thermo Scientific K-Alpha XPS system. Furthermore, the electrical characteristics of ITZO TFTs were measured under dark conditions at room temperature by using a Keithley 4200-SCS semiconductor analyzer.

3. RESULTS AND DISCUSSION

Figure 1a displays the GIXRD pattern of a 7.5 nm ITZO thin-film deposited on a glass substrate after annealing at 290 °C for 1 h in air. The broad peak observed could be attributed to the glass substrate. The GIXRD pattern did not reveal any characteristic peaks associated with the ITZO film, indicating its amorphous nature. The optical absorption spectrum was measured by using a UV−vis−NIR spectrometer to investigate the optical band gap of the ITZO film on a glass substrate after annealing at 290 °C for 1 h. The relationship between the bandgap of ITZO and the absorption coefficient is described by the following equation:[29]

$$(\alpha h\nu)^{1/n} = A(h\nu - E_g) \tag{1}$$

where α is the absorption coefficient, h is the Planck constant, ν is the incident photon frequency, E_g is the bandgap, and A is a constant. n = 1/2 for direct bandgap semiconductors or 2 for indirect bandgap semiconductors.[29] The ITZO films investigated in our study belong to the direct bandgap semiconductors. By extrapolating the absorption spectrum, the E_g of the ITZO film is determined to be 3.6 eV, as illustrated in Figure 1b.

Contact angle measurements were conducted to confirm the deposition of HMDS on ITZO and assess its influence on hydrophobicity. For contact angle measurements, the ITZO film was deposited on an SiO_2/Si substrate. A water contact angle of

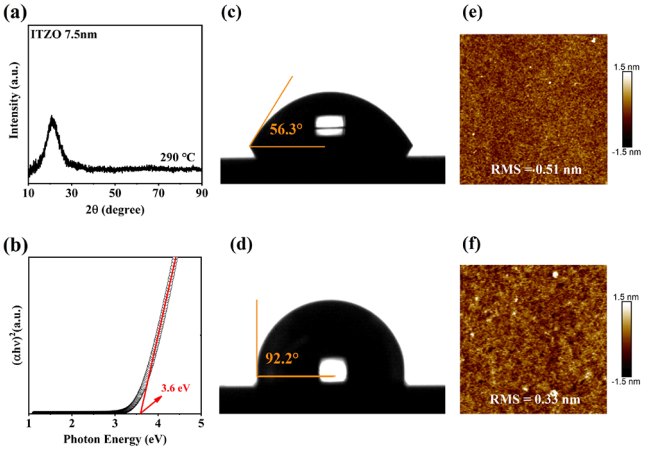

Figure 1. (a) GIXRD pattern of ITZO film deposited on a glass substrate after annealing at 290 °C for 1 h in air. (b) The band gap pattern of the ITZO thin film on a glass substrate after annealing at 290 °C. Profile images of water on (c) ITZO surface and (d) HMDS/ITZO. AFM images of the (e) ITZO surface on device A and (f) HMDS surface on device B.

56.3° was measured for the ITZO surface without the HMDS passivation layer, as shown in Figure 1c. In contrast, HMDS on ITZO yielded a water contact angle of 92.2°, as shown in Figure 1d.

The surface free energy (γ_ρ) is an important parameter for assessing the hydrophobicity of the HMDS-passivated surface, with a low γ_ρ indicating weak moisture attraction.[18] The relationship between surface-free energy and water contact angle can be expressed as

$$\gamma_\rho = \frac{\gamma_\omega}{4}(1 + \cos\theta)^2 \tag{2}$$

where γ_ω is the water surface free energy (73 mJ/m^2) and θ is the contact angle. The γ_ρ of the ITZO film without an HMDS passivation layer was determined to be 44.13 mJ/m^2, while the γ_ρ of HMDS on ITZO was determined to be 16.89 mJ/m^2. Prior to HMDS passivation, the ITZO surface exhibited hydrophilic properties (θ < 90°). However, after HMDS deposition, the surface became hydrophobic (θ > 90°) with a lower γ_ρ. As a result, the HMDS passivation layer effectively inhibits the absorption of moisture and oxygen molecules from the ITZO film.

AFM measurements were conducted both before and after HMDS passivation of the ITZO surface. Prior to HMDS passivation, the root-mean-square (RMS) surface roughness of ITZO surface on device A measured 0.51 nm, as shown in Figure 1e. However, after HMDS passivation, the RMS surface roughness on device B decreased to 0.33 nm, as shown in Figure 1f. Similar results, indicating an improvement in surface roughness after HMDS surface treatment, have been reported.[30]

Figure 2a shows schematic diagrams of two different device structures for ITZO TFTs. Device A represents an ITZO TFT without HMDS passivation, while Device B represents an ITZO TFT with HMDS passivation. The transfer characteristics of devices A and B are illustrated in Figure 2b,c.

The saturation mobility (μ_{sat}) and threshold voltage (V_{TH}) of the ITZO TFTs can be determined using the following equation:[31]

https://doi.org/10.1021/acsaelm.4c00100
ACS Appl. Electron. Mater. 2024, 6, 2442−2448

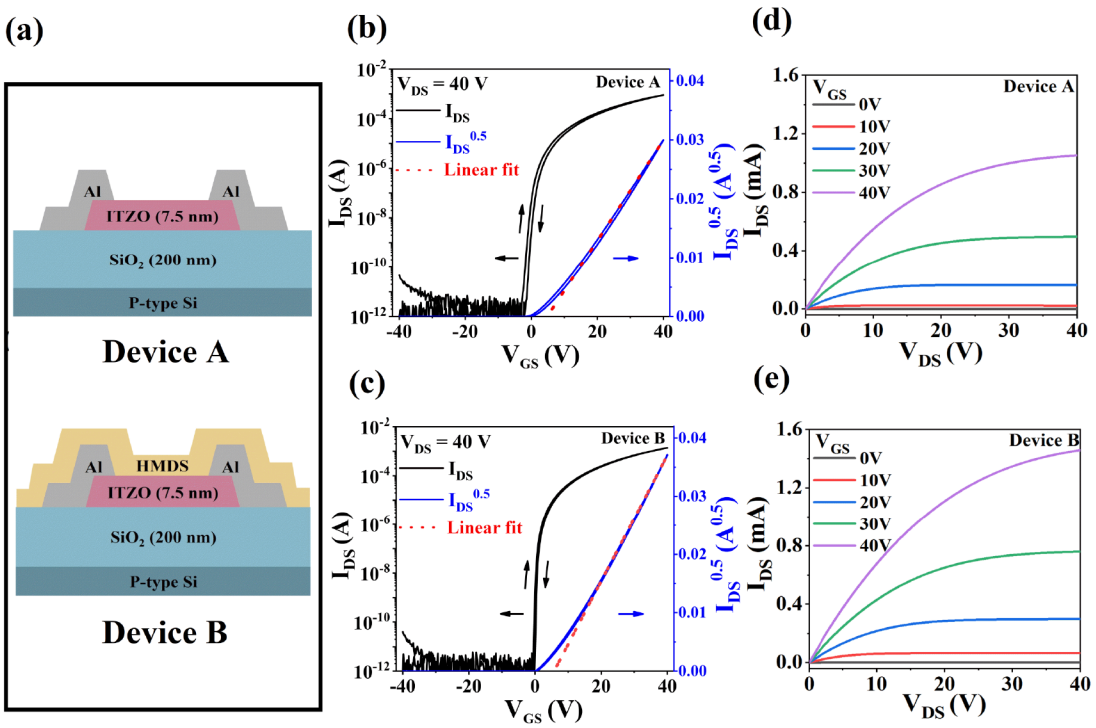

Figure 2. (a) Schematic diagram of two different device structures of ITZO TFTs: Device A is an ITZO TFT without HMDS passivation, and device B is an ITZO TFT with HMDS passivation. Transfer characteristics of (b) device A and (c) device B. Output characteristics of (d) device A and (e) device B.

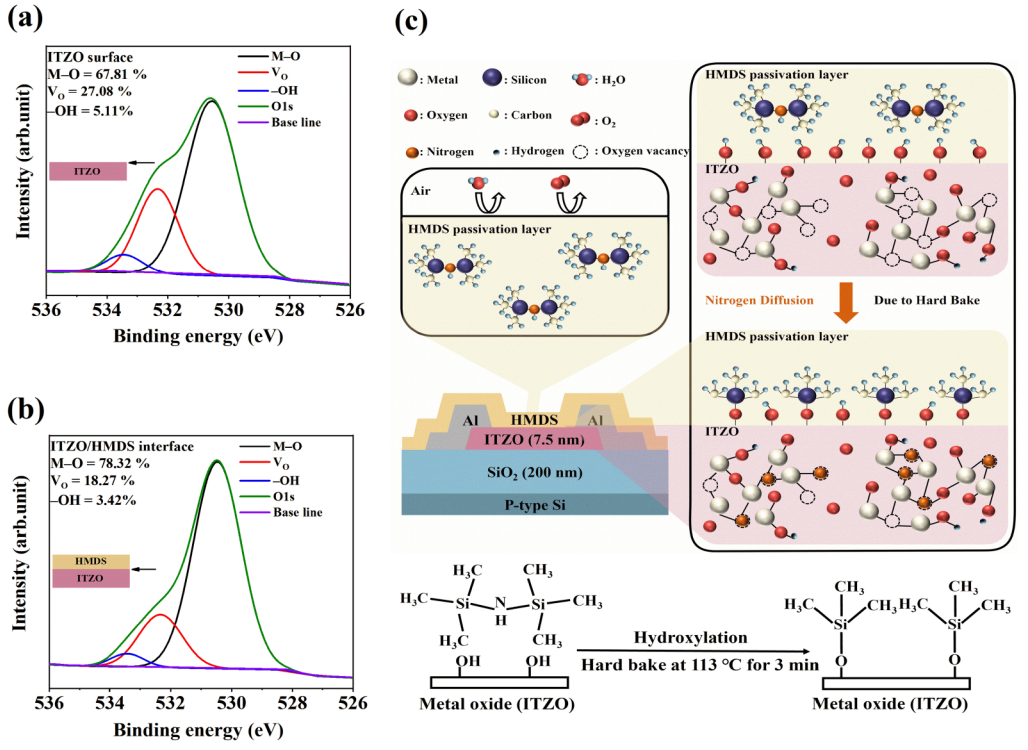

Figure 3. XPS O 1s spectral results of (a) ITZO surface and (b) HMDS/ITZO interface; (c) chemical reaction mechanisms of the HMDS passivation on the ITZO.

$$I_{DS} = \frac{C_{ox}\mu_{sat}W}{2L}(V_{GS} - V_{TH})^2 \quad (3)$$

where I_{DS} is drain current, C_{OX} is gate capacitance per unit area, and V_{GS} is gate voltage. Additionally, in Figure 2b,c, the square root of I_{DS} against V_{GS} is plotted, with V_{TH} approximated by determining the point of intersection between V_{GS} and the linear regression line of the square root of I_{DS}.

The interface trap density (N_{it}) can be estimated using the following equation:[12]

https://doi.org/10.1021/acsaelm.4c00100
ACS Appl. Electron. Mater. 2024, 6, 2442−2448

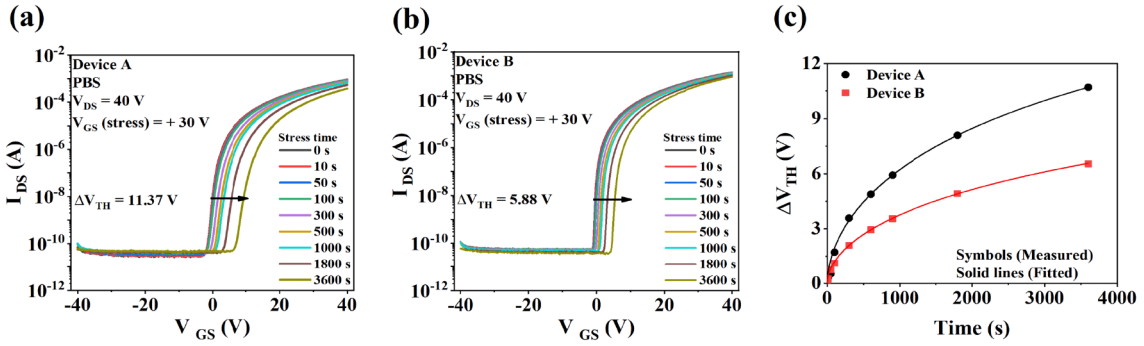

Figure 4. Transfer curves of ITZO TFTs under PBS for 3600 s: (a) ITZO TFT without HMDS passivation and (b) ITZO TFT with HMDS passivation. (c) ΔV_{TH} as a function of stress time under PBS, with the stress condition set at V_{GS} (stress) = +30 V.

$$N_{it} = \left[\frac{\text{S.S}\log(e)}{\text{kT}/q} - 1\right] \times \frac{C_{ox}}{q^2}$$

where k is Boltzmann's constant, T is the temperature, q is the electron charge, and the S.S is subthreshold swing. The S.S can be estimated from the transfer curve by determining the minimum V_{GS} required to increase I_{DS} by one decade.[32]

Device A exhibits μ_{sat} of 16.86 $cm^2 \cdot V^{-1} \cdot s^{-1}$, V_{TH} of 5.54 V, S.S of 0.59 $V \cdot dec^{-1}$, N_{it} of 9.5×10^{11} $cm^{-2} \cdot eV^{-1}$, and on/off current ratio (I_{on}/I_{off}) of 3×10^8. In comparison, device B exhibits μ_{sat} of 27.01 $cm^2 \cdot V^{-1} \cdot s^{-1}$, V_{TH} of 6.42 V, S.S of 0.22 $V \cdot dec^{-1}$, N_{it} of $2.9 \times 10^{11} cm^{-2} \cdot eV^{-1}$, and I_{on}/I_{off} of 9×10^8. Thus, HMDS passivation on an ITZO TFT improves the electrical performance. In both devices, the gate leakage current, I_{GS}, is found to be less than 0.1 nA (see Figure S2). Figure 2d,e shows the output characteristics of devices A and B, where both devices operate in the n-type enhancement mode.

XPS measurements were conducted on the ITZO films of both devices A and B to establish a correlation between the binding energy and device performance. Figure 3a,b shows the O 1s core-level XPS spectra of the ITZO film surface for device A and the interface between the ITZO film and the HMDS passivation layer for device B. The XPS spectra are deconvoluted into three subpeaks: metal-oxide (M−O) bonding at 530.60 eV, oxygen vacancy (V_o) at 532.50 eV, and hydroxyl (−OH) at 533.58 eV, using Gaussian−Lorentzian deconvolution.[10] At the ITZO/HMDS interface, the concentration of M−O bonding increases from 67.81 to 78.32%, while the concentration of V_o and −OH decreases from 27.08 to 18.2% and from 5.11 to 3.42%, respectively, due to passivation. Consequently, HMDS passivation increases the concentration of M−O and reduces the concentration of V_o and −OH, contributing to enhanced electrical performance of device B.[10,12] This phenomenon is plausibly explained by the chemical reaction mechanisms of HMDS passivation, as depicted in Figure 3c. When HMDS is applied to the ITZO surface, it reacts with the −OH groups on the ITZO to form silicon−oxygen (Si−O) bonds.[33] Furthermore, this reaction leads to the release of ammonia and nitrogen (N) atoms diffusing into the ITZO channel.[18] These N atoms can partially occupy the oxygen-deficient sites, thereby suppressing the formation of V_o.[18] As a result, HMDS passivation decreases the concentration of V_o and − OH, which justifies the increase in the concentration of M−O. The enhanced mobility of device B can be attributed to an increased concentration of M−O, leading to an improved conduction pathway in the channel.[34,35] In addition, device B exhibits fewer defects, including a reduced concentration of V_o and −OH, further contributing to its overall enhanced performance.[12]

To test the electrical stability of ITZO TFTs, a positive bias stress (PBS) of V_{GS} (stress) = +30 V was applied to device A and device B for 3600 s under atmospheric conditions. Transfer characteristics were obtained by sweeping V_{GS} from = −40 to 40 V with V_{DS} = 40 V. The transfer characteristics of both devices A and B under PBS are shown in Figure 4a,b. After the PBS of 3600 s, we observed the threshold voltage change (ΔV_{TH}) for device A and device B, which was found to be +11.37 and +5.88 V, respectively. Device B clearly exhibits enhanced PBS stability compared to device A, primarily due to a lower defect concentration in the channel layer, including a reduced concentration of V_o and −OH.[12] Additionally, the HMDS passivation layer effectively shields the ITZO active channel layer from exposure to oxygen and moisture in the air, thereby enhancing the PBS stability.

Figure 4c shows the ΔV_{TH} of devices with respect to stress time under PBS. These data were fitted using a stretched-exponential equation:[12]

$$\Delta V_{TH} = \Delta V_{TH0}\{1 - \exp[-(t/\tau)^{\beta}]\} \quad (4)$$

where ΔV_{TH0} is the ΔV_{TH} at infinite stressing time, t is the stress time, τ is the characteristic trapping time, and β is the stretched-exponential exponent. Figure 4c shows that the stress time dependence of ΔV_{TH} under PBS is well fitted with the exponential equation, suggesting that carrier trapping is the main degradation mechanism.[36] The τ values of device A and device B are 5935 and 10 000 s, respectively. Device B exhibits a higher τ than device A, indicating a reduced defects concentration in the channel.[12]

To investigate uniformity and reproducibility, we extracted electrical characteristics from an additional set of 8 devices for both ITZO TFTs without and with HMDS passivation. Their transfer characteristics are depicted in Figure 5a,b, while statistical data for μ_{sat}, S.S, and V_{TH} are displayed in Figure 5c. These data clearly indicate that ITZO TFTs with HMDS passivation exhibit enhanced electrical performance compared to those without HMDS passivation. Specifically, ITZO TFTs without HMDS passivation exhibit μ_{sat} of 16.82 ± 0.42 $cm^2 \cdot V^{-1} \cdot s^{-1}$, S.S of 0.70 ± 0.12 $V \cdot dec^{-1}$, V_{TH} of 5.64 ± 0.41 V, and I_{on}/I_{off} of 3×10^8. In contrast, ITZO TFTs with HMDS passivation exhibit μ_{sat} of 26.15 ± 1.14 $cm^2 \cdot V^{-1} \cdot s^{-1}$, S.S of 0.26 ± 0.04 $V \cdot dec^{-1}$, V_{TH} of 6.21 ± 0.71 V, and I_{on}/I_{off} of 9×10^8.

In addition, long-term stability assessments were conducted for devices A and B, involving initial electrical measurements immediately after fabrication and subsequent measurements

https://doi.org/10.1021/acsaelm.4c00100
ACS Appl. Electron. Mater. 2024, 6, 2442−2448

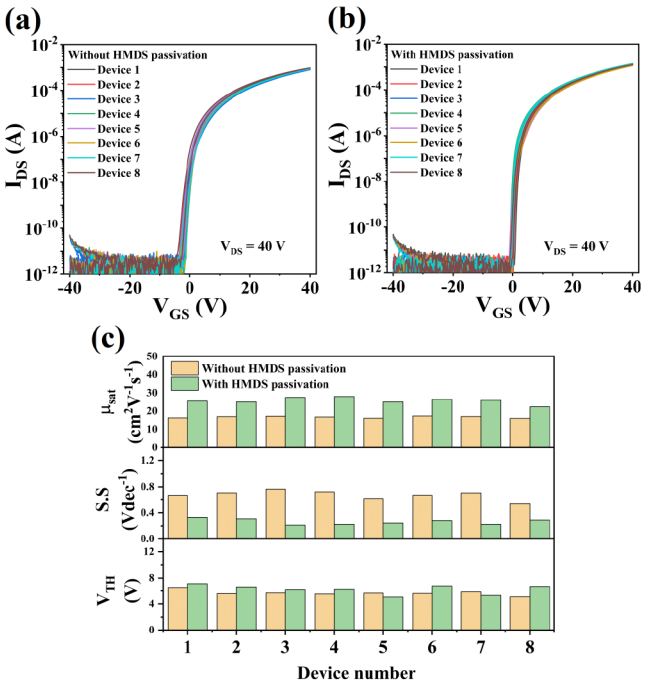

Figure 5. Transfer characteristics of ITZO TFTs (a) without HMDS passivation and (b) with HMDS passivation. (c) Statistical data of saturation mobility, subthreshold swing, and threshold voltage of ITZO TFTs.

after a 6-month storage period under ambient conditions. Figure 6 displays the resulting transfer characteristics for their long-term stability. Device B demonstrates favorable long-term stability, with minor changes in performance observed after 6 months. Specifically, μ_{sat} changed from 27.01 to 25.60 $cm^2 \cdot V^{-1}$.

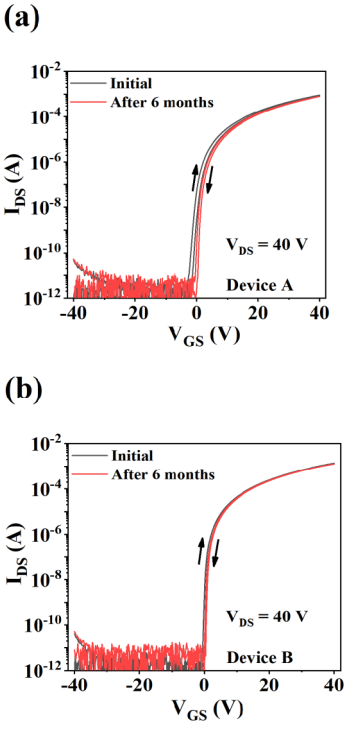

Figure 6. Transfer characteristics of (a) device A and (b) device B before and after storage in ambient air for 6 months.

s^{-1}, V_{TH} changed from 6.42 to 5.31 V, and S.S changed from 0.22 to 0.24 V·dec^{-1}. In contrast, device A exhibits significant changes in performance after 6 months, Specifically, μ_{sat} changed from 16.86 to 13.72 $cm^2 \cdot V^{-1} \cdot s^{-1}$, V_{TH} changed from 5.54 to 5.63 V, and S.S changed from 0.59 to 0.35 V·dec^{-1}. The electrical properties of device B are more stable over 6 months, suggesting the formation of an effective passivation layer through HMDS treatment.

Various passivation layers, including organic, inorganic, and organic/inorganic hybrid options have been applied to ITZO TFTs, leading to enhanced electrical performance and stability consistent with our findings.[9,14,15,18,19,37] Notably, our spin-coated HMDS passivation layer stands out as a cost-effective alternative among the various organic-solution-based passivation layers. HMDS passivation layers exhibit a similar ability to react with −OH groups as other organic self-assembled monolayer passivation layers, such as *n*-octyltriethoxysilane and *n*-octadecyltrichlorosilane.[14,26] The application of HMDS passivation is expected to be a viable approach for enhancing the electrical performance and bias stability of oxide semiconductor TFTs through a chemical reaction with surface −OH groups.

4. CONCLUSIONS

In this work, we present the fabrication and characterization of high performance ITZO TFTs with HMDS passivation. The experimental results clearly illustrate that HMDS passivation significantly improves the electrical performance and stability of the ITZO TFTs. XPS analysis reveals that these enhancements in device performance and stability are mainly attributed to an increased concentration of M−O and a reduced concentration of V_o and −OH in the active ITZO channel layer. Additionally, the HMDS passivation layer effectively shields the ITZO active channel layer from exposure to oxygen and moisture in the air, further enhancing the device's PBS stability. Consequently, ITZO TFTs with HMDS passivation exhibit a saturation mobility of 26.15 ± 1.14 $cm^2 \cdot V^{-1} \cdot s^{-1}$, subthreshold swing of 0.26 ± 0.04 V·dec^{-1}, and an on/off current ratio of 9×10^8. Furthermore, HMDS is expected to react effectively with surface −OH groups on other oxide semiconductor materials, forming passivation layers that can enhance the device's electrical performance and bias stability in a similar manner. This work demonstrates the potential of spin-coated HMDS as a passivation strategy for oxide semiconductor TFTs in next-generation displays.

■ ASSOCIATED CONTENT

Supporting Information

The Supporting Information is available free of charge at https://pubs.acs.org/doi/10.1021/acsaelm.4c00100.

ITZO TFT fabrication process; Transfer characteristics and gate leakage current of ITZO TFTs (PDF)

■ AUTHOR INFORMATION

Corresponding Authors

Jidong Jin − *Department of Photonics and Nanoelectronics, Hanyang University, Ansan 15588, Republic of Korea;* orcid.org/0000-0002-8400-0053; Email: jinjidong@hanyang.ac.kr

Younghyun Kim − *Department of Photonics and Nanoelectronics and BK21 FOUR ERICA-ACE Center, Hanyang University, Ansan 15588, Republic of Korea;*

https://doi.org/10.1021/acsaelm.4c00100
ACS Appl. Electron. Mater. 2024, 6, 2442−2448

orcid.org/0000-0001-8072-1251;
Email: younghyunkim@hanyang.ac.kr

Authors

Xinkai Sun − *Department of Photonics and Nanoelectronics and BK21 FOUR ERICA-ACE Center, Hanyang University, Ansan 15588, Republic of Korea*

Jae-Hoon Han − *Center for Opto-Electronic Materials and Devices, Korea Institute of Science and Technology (KIST), Seoul 02792, Republic of Korea;* orcid.org/0000-0003-3575-9140

Zhenyuan Xiao − *Department of Photonics and Nanoelectronics and BK21 FOUR ERICA-ACE Center, Hanyang University, Ansan 15588, Republic of Korea;* orcid.org/0000-0003-2996-7162

Simin Chen − *Department of Photonics and Nanoelectronics and BK21 FOUR ERICA-ACE Center, Hanyang University, Ansan 15588, Republic of Korea*

Taewon Jin − *Department of Photonics and Nanoelectronics and BK21 FOUR ERICA-ACE Center, Hanyang University, Ansan 15588, Republic of Korea*

Taehyeon Noh − *Department of Photonics and Nanoelectronics and BK21 FOUR ERICA-ACE Center, Hanyang University, Ansan 15588, Republic of Korea*

Seoungmin Park − *Department of Photonics and Nanoelectronics and BK21 FOUR ERICA-ACE Center, Hanyang University, Ansan 15588, Republic of Korea*

Jaekyun Kim − *Department of Photonics and Nanoelectronics and BK21 FOUR ERICA-ACE Center, Hanyang University, Ansan 15588, Republic of Korea;* orcid.org/0000-0001-9726-8166

Complete contact information is available at:
https://pubs.acs.org/10.1021/acsaelm.4c00100

Author Contributions

[‖]X.S. and J.-H.H. contributed equally to this paper.

Notes

The authors declare no competing financial interest.

■ ACKNOWLEDGMENTS

This research was supported in part by the Technology Innovation Program through the Korea Evaluation Institute of Industrial Technology (KEIT), funded by the Ministry of Trade, Industry & Energy (MOTIE, Korea) under grant 20015909; in part by the Korea Basic Science Institute (National research Facilities and Equipment Center), grant funded by the Ministry of Education, under grant 2023R1A6C103A035 and grant 2021R1A6C101A405; in part by the National Research Foundation of Korea (NRF) grant founded by the Korea government (MSIT) under grant NRF-2023R1A2C1007034; in part by the KIST institutional project under grant 2E32942; and in part by the research fund of Hanyang University under grant HY-2021-2716.

■ REFERENCES

(1) Sheng, J.; Jeong, H.-J.; Han, K.-L.; Hong, T.; Park, J.-S. Review of Recent Advances in Flexible Oxide Semiconductor Thin-Film Transistors. *J. Inf. Disp.* **2017**, *18* (4), 159−172.

(2) Ide, K.; Nomura, K.; Hosono, H.; Kamiya, T. Electronic Defects in Amorphous Oxide Semiconductors: A Review. *Phys. Status Solidi A* **2019**, *216* (5), 1800372.

(3) Shim, G. W.; Hong, W.; Cha, J. H.; Park, J. H.; Lee, K. J.; Choi, S. Y. TFT Channel Materials for Display Applications: From Amorphous Silicon to Transition Metal Dichalcogenides. *Adv. Mater.* **2020**, *32* (35), 1907166.

(4) Shi, J.; Zhang, J.; Yang, L.; Qu, M.; Qi, D. C.; Zhang, K. H. Wide Bandgap Oxide Semiconductors: from Materials Physics to Optoelectronic Devices. *Adv. Mater.* **2021**, *33* (50), 2006230.

(5) Shiah, Y.-S.; Sim, K.; Shi, Y.; Abe, K.; Ueda, S.; Sasase, M.; Kim, J.; Hosono, H. Mobility−Stability Trade-Off in Oxide Thin-Film Transistors. *Nat. Electron.* **2021**, *4* (11), 800−807.

(6) Xiao, Z.; Jin, J.; Lee, J.; Choi, G.; Lin, X.; Zhang, J.; Kim, J. Improved Performance and Bias Stability of Indium-Tin-Zinc-Oxide Thin-Film Transistors Enabled by an Oxygen-Compensated Capping Layer. *Phys. Status Solidi A* **2024**, *221* (2), 2300544.

(7) Shi, Y.; Shiah, Y.-S.; Sim, K.; Sasase, M.; Kim, J.; Hosono, H. High-Performance a-ITZO TFTs with High Bias Stability Enabled by Self-Aligned Passivation Using a-GaO_x. *Appl. Phys. Lett.* **2022**, *121*, 212101.

(8) Sheng, J.; Han, J.-H.; Choi, W.-H.; Park, J.; Park, J.-S. Performance and Stability Enhancement of In−Sn−Zn−O TFTs Using SiO_2 Gate Dielectrics Grown by Low Temperature Atomic Layer Deposition. *ACS Appl. Mater. Interfaces* **2017**, *9* (49), 42928−42934.

(9) Zhong, W.; Kang, L.; Deng, S.; Lu, L.; Yao, R.; Lan, L.; Kwok, H. S.; Chen, R. Effect of Sc_2O_3 Passivation Layer on the Electrical Characteristics and Stability of InSnZnO Thin-Film Transistors. *IEEE Trans. Electron Devices* **2021**, *68* (10), 4956−4961.

(10) Lee, J.; Jin, J.; Maeng, S.; Choi, G.; Kim, H.; Kim, J. Enhancement of the Electrical Performance and Bias Stability of RF-Sputtered Indium Tin Zinc Oxide Thin-Film Transistors with Vertical Stoichiometric Oxygen Control. *ACS Appl. Electron. Mater.* **2022**, *4* (4), 1800−1806.

(11) Nakata, M.; Zhao, C.; Kanicki, J. DC Sputtered Amorphous In−Sn−Zn−O Thin-Film Transistors: Electrical Properties and Stability. *Solid-State Electron.* **2016**, *116*, 22−29.

(12) Jin, J.; Lin, X.; Zhang, J.; Lee, J.; Xiao, Z.; Lee, S.; Kim, J. L.-V. High-Performance, Indium-Tin-Zinc-Oxide Thin-Film Transistors Based on Dual-Channel and Anodic-Oxide. *Adv. Electron. Mater.* **2023**, *9* (3), 2201117.

(13) Chen, F.; Zhang, M.; Wan, Y.; Xu, X.; Wong, M.; Kwok, H.-S. Advances in Mobility Enhancement of ITZO Thin-Film Transistors: A Review. *J. Semicond.* **2023**, *44* (9), 091602.

(14) Zhong, W.; Yao, R.; Liu, Y.; Lan, L.; Chen, R. Effect of Self-Assembled Monolayers (SAMs) as Surface Passivation on the Flexible a-InSnZnO Thin-Film Transistors. *IEEE Trans. Electron Devices* **2020**, *67* (8), 3157−3162.

(15) Zhong, W.; Li, G.; Lan, L.; Li, B.; Chen, R. InSnZnO Thin-Film Transistors With Vapor-Phase Self-Assembled Monolayer as Passivation Layer. *IEEE Electron Device Lett.* **2018**, *39* (11), 1680−1683.

(16) Zhong, W.; Li, G.; Lan, L.; Li, B.; Chen, R. Effects of Annealing Temperature on Properties of InSnZnO Thin Film Transistors Prepared by Co-sputtering. *RSC Adv.* **2018**, *8* (61), 34817−34822.

(17) Kim, D.; Yoon, S.; Jeong, Y.; Kim, Y.; Kim, B.; Hong, M. Role of Adsorbed H_2O on Transfer Characteristics of Solution-Processed Zinc Tin Oxide Thin-Film Transistors. *Appl. Phys. Express* **2012**, *5* (2), 021101.

(18) Chen, Y.; Li, B.; Zhong, W.; Li, G.; Lu, L.; Zhou, C.; Lan, L.; Chen, R. InSnZnO Thin-Film Transistors With Nitrogenous Self-Assembled Multilayers Passivation. *IEEE Trans. Electron Devices* **2021**, *68* (11), 5612−5617.

(19) Zhong, W.; Yao, R.; Chen, Z.; Lan, L.; Chen, R. Self-Assembled Monolayers (SAMs)/Al_2O_3 Double Layer Passivated InSnZnO Thin-Film Transistor. *IEEE Access* **2020**, *8*, 101834−101839.

(20) Chen, Y.; Li, B.; Zhong, W.; Luo, D.; Li, G.; Zhou, C.; Lan, L.; Chen, R. Effect of Head Groups in Self-Assembled Monolayer Passivation on Properties of InSnZnO Thin-Film Transistors. *IEEE Trans. Electron Devices* **2022**, *69* (1), 160−165.

(21) Chen, R.; Lan, L. Solution-Processed Metal-Oxide Thin-Film Transistors: A Review of Recent Developments. *Nanotechnology* **2019**, *30* (31), 312001.

(22) Corsino, D. C.; Bermundo, J. P. S.; Fujii, M. N.; Takahashi, K.; Ishikawa, Y.; Uraoka, Y. Bias Stress and Humidity Exposure of Amorphous InGaZnO Thin-Film Transistors with Atomic Layer

Deposited Al_2O_3 Passivation Using Dimethylaluminum Hydride at 200 °C. *J. Phys. D* **2020**, *53* (16), 165103.
(23) Hong, S.; Park, S. P.; Kim, Y.-G.; Kang, B. H.; Na, J. W.; Kim, H. J. Low-Temperature Fabrication of an HfO_2 Passivation Layer for Amorphous Indium−Gallium−Zinc Oxide Thin Film Transistors Using a Solution Process. *Sci. Rep.* **2017**, *7* (1), 16265.
(24) Aman, S. M.; Koretomo, D.; Magari, Y.; Furuta, M. Influence of Deposition Temperature and Source Gas in PE-CVD for SiO_2 Passivation on Performance and Reliability of In−Ga−Zn−O Thin-Film Transistors. *IEEE Trans. Electron Devices* **2018**, *65* (8), 3257−3263.
(25) Yatsu, K.; Lee, H.-A.; Park, I.-J.; Kwon, H.-I. Effects of High-Energy X-ray Irradiation on the Electrical and Chemical Properties of In−Ga−Sn−O Thin Films with Al_2O_3 Passivation Layer for Thin-Film Transistor Applications. *ACS Appl. Electron. Mater.* **2023**, *5* (5), 2528−2537.
(26) Cai, W.; Wilson, J.; Zhang, J.; Brownless, J.; Zhang, X.; Majewski, L. A.; Song, A. Significant Performance Enhancement of Very Thin InGaZnO Thin-Film Transistors by a Self-Assembled Monolayer Treatment. *ACS Appl. Electron. Mater.* **2020**, *2* (1), 301−308.
(27) Yue, D.; Feng, Q.; Huang, X.; Zhang, X.; Chen, H. In Situ Fabrication of a Superhydrophobic ORMOSIL Coating on Wood by an Ammonia−HMDS Vapor Treatment. *Coatings* **2019**, *9* (9), 556.
(28) Lim, S. C.; Kim, S. H.; Lee, J. H.; Kim, M. K.; Kim, D. J.; Zyung, T. Surface-Treatment Effects on Organic Thin-Film Transistors. *Synth. Met.* **2005**, *148* (1), 75−79.
(29) Weng, L.; Zhang, S.; Kuang, D.; Liu, B.; Liu, X.; Jiang, B.; Zhang, G.; Bao, Z.; Ning, C.; Shi, D.; Guo, J. Performance Improvement of Amorphous Thin-Film Transistors With Solution-Processed InZnO/InMgZnO Bilayer Channels. *IEEE Trans. Electron Devices* **2023**, *70* (8), 4186−4193.
(30) Yan, Y.; Liu, J.; Zhang, B.; Xia, R.; Zhang, Y.; Guan, Z. Enhanced Mechanical and Hydrophobic Antireflective Nanocoatings Fabricated on Polycarbonate Substrates by Combined Treatment of Water and HMDS Vapor. *Materials* **2023**, *16* (10), 3850.
(31) Moreira, M.; Carlos, E.; Dias, C.; Deuermeier, J.; Pereira, M.; Barquinha, P.; Branquinho, R.; Martins, R.; Fortunato, E. Tailoring IGZO Composition for Enhanced Fully Solution-Based Thin Film Transistors. *Nanomater* **2019**, *9* (9), 1273.
(32) Cai, W.; Li, H.; Zang, Z. O.-V. One-Volt, Solution-Processed InZnO Thin-Film Transistors. *IEEE Electron Device Lett.* **2021**, *42* (4), 525−528.
(33) Gun'ko, V.; Vedamuthu, M.; Henderson, G.; Blitz, J. Mechanism and Kinetics of Hexamethyldisilazane Reaction with A Fumed Silica Surface. *J. Colloid Interface Sci.* **2000**, *228* (1), 157−170.
(34) Bukke, R. N.; Avis, C.; Jang, J. Solution-Processed Amorphous In−Zn−Sn Oxide Thin-Film Transistor Performance Improvement by Solution-Processed Y_2O_3 Passivation. *IEEE Electron Device Lett.* **2016**, *37* (4), 433−436.
(35) Mude, N. N.; Bukke, R. N.; Saha, J. K.; Avis, C.; Jang, J. H. S. Highly Stable, Solution-Processed Ga-Doped IZTO Thin Film Transistor by Ar/O_2 Plasma Treatment. *Adv. Electron. Mater.* **2019**, *5* (12), 1900768.
(36) Kang, D. H.; Kang, I.; Ryu, S. H.; Ahn, Y. S.; Jang, J. Effect of SiO_2 and/or SiN_x Passivation Layer on Thermal Stability of Self-Aligned Coplanar Amorphous Indium−Gallium−Zinc−Oxide Thin-Film Transistors. *J. Disp. Technol.* **2013**, *9* (9), 699−703.
(37) Lin, D.; Li, X.; Zhong, W.; Zhou, C.; Lan, L.; Chen, R. Enhanced Electrical and Mechanical Performance of InSnZnO TFTs With Multifunctional Laminated Organic Passivation Layer. *IEEE Trans. Electron Devices* **2022**, *69* (11), 6146−6153.

https://doi.org/10.1021/acsaelm.4c00100
ACS Appl. Electron. Mater. 2024, 6, 2442−2448